SPACE TELESCOPE SCIENCE INSTITUTE
Operated for NASA by AURA

Instrument Science Report ACS 2006-01

PSFs, Photometry, and Astrometry for the ACS/WFC

Jay Anderson

jay@eeyore.rice.edu

Ivan R. King

king@astro.washington.edu

February 2006

Abstract

We develop and present effective PSFs for the F606W filter in the WFC, and then for five other filters. After briefly reviewing the concept of the effective PSF, we show that the WFC PSF varies with position in the detector. We represent the PSF by a 9×10 array of fiducial PSFs, between which a tailor-made PSF is to be interpolated for each star. Fitting these PSFs to star images gives photometry and astrometry with accuracies of 0.01 mag and 0.01 pixel, respectively, for well-exposed star images. We study short-term variability of the PSF and also study it over the history of ACS. The variability with time depends mainly on focus, and can be represented as a spatially fixed "perturbation PSF" for each image. We make `FORTRAN` programs available for generating our PSFs, for measuring star images with them, and for a number of related utility tasks.

1. Introduction

In a previous report (Anderson 2003) we used a spatially constant PSF for astrometry, and succeeded in measuring better positions with ACS/WFC than we had been able to do with WFPC2. But we soon discovered that spatial variations in the PSF were weakening the astrometry and were badly hurting photometry.

The following sections present our modeling of the F606W PSF, and also provide PSFs for other filters. In Sec. 2 we begin with a short tutorial on the effective PSF. In Sec. 3 we examine the spatial scale of PSF variation and develop a scheme for dealing with it, and in Sec. 4 we look into short-term and long-term time variations. Finally, Sec. 5 describes some software tools for measuring stars; these tools are also useful in more advanced analyses.

1.1. A word about images

All of the PSFs shown here, and the routines provided here, are designed to work on the `_flt` images. These images have been bias-subtracted and flat-fielded, but have not been resampled, and are therefore the most direct observations that we have of the astronomical scene. By contrast, positions or fluxes from PSF-fitting on the individual-exposure `_drz` images can result in systematic errors as large as 0.05 pixel or 0.05 magnitude. The latter images are adequate for aperture photometry with generous apertures, but one cannot always afford such large apertures for faint or crowded stars. Astrometry on individual drizzled images should be avoided.

We note that PSF-fit photometry on drizzled associations can be done accurately, provided sufficient sub-pixel dithers were used, combined with accurate image-to-image registrations to suppress sensitivity to sub-pixel phase errors.

1.2. Data sets used

We use three data sets here:

- GO-10424 took 126 orbits on an outer field of the globular cluster NGC 6397, through F606W and F814W. There are about 4000 well-exposed stars, and the many exposures provide a good study of the short-term behavior of the PSF.
- GO-10252 observed a moderately dense field in Omega Cen on 11 December 2004 for the purpose of deriving high-accuracy PSFs and distortion solutions for the

most-used WFC filters, F606W and F814W. Unfortunately these observations were taken just before a major focus readjustment on 22 Dec 2004, so that the PSF is not at all typical of that for most ACS observations. Thus instead of using these data to calibrate normal WFC operation, we use them to examine how accurately our calibrations work in an extreme circumstance.

- The outer calibration field in 47 Tuc, ∼5 arc minutes west of the cluster center, has been observed over 300 times by the WFC (more than 160 times through F606W), and gives a good handle on the long-term behavior of the PSF. In a forthcoming ISR we will also use this data set to study the accuracy and stability of the distortion solution.

2. The effective PSF

We give here a brief description of our approach to the modeling of PSFs. More background and details can be found for WFPC2 in Anderson & King 2000 (AK00), and for the HRC in Anderson & King 2004.

The PSF in CCD images derives from two functions, neither of which is observed directly: The instrumental PSF gives the flux for a point source as a function of offset from its center, and the pixel response function gives the sensitivity at each point within a pixel. There is a way of looking at the PSF, however, that bypasses any need to know either of these functions explicitly. When Alexander the Great was confronted with the Gordian knot, which others had failed to untie, his solution was to draw his sword and cut through it. Our Gordian solution to the PSF problem is the effective PSF. This is a continuous function of $(\Delta x, \Delta y)$, the offset from the center of the PSF, whose value at any point is the fraction of the light of a point source that would fall in a pixel centered at that point. The ePSF, as we shall call it, tells us everything that we need to know about the PSF. It is far easier to use than any other representation of the PSF, since it requires no integration and no explicit use—or even knowledge—of either the instrumental PSF or the pixel response function.

Rather than force it into an analytic mold, we shall treat the ePSF in a purely empirical manner and simply tabulate its value at an array of points. We have found that with a spacing of 0.25 of a pixel unit, bi-cubic interpolation gives sufficient accuracy.

If a star with flux f_* is centered at (x_*, y_*), on a background whose level is s_*, then the expected flux in pixel (i, j) is

$$\begin{aligned} P_{ij} &= f_* \cdot \psi_{\rm E}(\Delta x, \Delta y) + s_* \\ &= f_* \cdot \psi_{\rm E}(i - x_*, j - y_*) + s_*, \end{aligned} \tag{1}$$

where $\psi_{\rm E}$ is the ePSF. The same equation is used in the derivation of the PSF; each pixel in each star image provides an estimate at a point in the ePSF:

$$\hat{\psi}_{\rm E}(i - x_*, j - y_*) = \frac{P_{ij} - s_*}{f_*}. \tag{2}$$

2.1. Converging on a PSF model

Thus we use the PSF to find positions and fluxes, and we use positions and fluxes to derive the PSF. This may sound like circular reasoning, but in fact, iteration of the two

processes rapidly converges to a good ePSF, provided we have a well-dithered set of images. AK00 and Anderson & King 2004 discuss this process in detail.

Our WFPC2 PSFs in AK00 covered only the inner 5×5 pixels of a star. The WFC has a much larger dynamic range, and a better-sampled PSF, so it makes sense to construct PSFs that extend farther out; ours will go out 12.5 pixel units in each direction. Our 4×-supersampled PSFs will thus be tables of 101×101 entries, centered at [51,51]. We emphasize again that the ePSF is a continuous function, and that the quarter-pixel interval is only that of the tabulation. We could just as well have tabulated the ePSF at an interval of, say, 0.234 pixel—but it would not have been nearly as convenient. As we have said, bi-cubic interpolation yields accurate ePSF values between the grid points.

Now that we have prescriptions for specifying, constructing, and evaluating the effective PSF, we turn to the question of spatial variability.

2.2. An aside about the pixel-response function.

Although the effective-PSF approach does not need to treat either the instrumental PSF or the pixel-response function individually, it can still be instructive to consider how these functions may impact our PSFs.

As we mentioned above, the ePSF is the convolution of the instrumental PSF with the pixel-response function of the detector:

$$\psi_{\rm E} = \psi_{\rm I} \otimes \Pi_{\rm CCD}.$$

The pixel-response function of the detector actually has two contributions: (1) the intra-pixel-sensitivity function and (2) charge diffusion, so it can be written:

$$\Pi_{\rm CCD}(i,j) = \Pi_{\rm pix} \otimes \delta_{\rm diff}(i,j).$$

The intra-pixel-sensitivity function $\Pi_{\rm pix}$ is non-zero only for Δx and Δy between -0.5 and 0.5, but it should have the same shape for all pixels across the detector. For uniformly responsive pixels, this will be a perfect top-hat Π function. For pixels that have sensitivity variations, $\Pi_{\rm pix}$ will be less than 1.0 at some pixel phases. The diffusion term $\delta_{\rm diff}$ will be a true delta function if there is no diffusion (electrons end up exactly where they are generated). But if there is diffusion it will have some broadness, which means that an electron may end up in one pixel after being generated in another. We have written it $\delta_{\rm diff}$ as a function of location on the chip to underline the fact that the diffusion properties change with chip thickness.

We will find below that much of the variation of the ePSFs comes from the variation of diffusion across the chip. It does not matter to us whether the changes in the shape of the ePSF come from diffusion variations or variations in the optics-based $\psi_{\rm I}$. It is only important that our model for $\psi_{\rm E}$ properly track these variations.

In Sec. 3.1.3 we will make use of the fact that the WFC pixels are uniformly responsive ($\Pi_{\rm pix} = \Pi$) in order to simplify our PSF-construction procedure. An ISR on this is in preparation.

2.3. The radial extent of our PSFs

Our PSF models formally go out to a radius of 12.5 image pixels. Unsaturated stars have a small amount of signal this far out, and it is good to be able to subtract them relatively cleanly when searching for faint objects. Also, when evaluating whether a faint bump next to a brighter star is real, a model of the extended PSF can be quite useful.

Unsaturated stars do not, however, have enough signal beyond about 8 pixels to constrain the PSF accurately, so we use saturated stars to do this. We measure fluxes and postions of the brightest stars in short exposures, and this allows us to know their flux and position in the deeper images, where they are saturated, but where their wings have plenty of signal. Such a bootstrapping method is not as accurate as when we measure all parts of the PSF simultaneously for the same stars, but the procedure does allow to us arrive at a decent model for the PSF outskirts.

There are generally not enough saturated stars in an image to explore how the PSF halo may vary with position on the chip, so we construct a single model of the halo and graft it onto the inner part of the PSF, which changes from place to place on the chip. This grafting is done between 6 and 8 pixels, so that within 6 pixels, the PSF is entirely locally determined from the unsaturated stars, and beyond 8 pixels the PSF is the same across the chip, coming from the global model from the saturated stars. Therefore, our PSFs will be most accurate within 6 pixels, but should still provide a handle on the PSF beyond this radius.

3. The spatial variation of the PSF

Because of position-dependent charge diffusion and, to a lesser extent, optical aberrations, the WFC PSF changes shape with location on the detector. We will treat this spatial variability in a way similar to our treatment of WFPC2 PSFs in AK00, deriving fiducial PSFs at a number of specific points in the chips. To measure a star at any given location in the detector, we will interpolate in this array of fiducial PSFs.

The first step is to determine how dense a network of points is needed in order to represent the spatial variations of the PSF. Toward this end, we fit a spatially constant PSF to stars throughout the detector, and examine the residuals.

Figure 1 shows the residual for the central pixel of each star in a set of F606W images, after fitting the same PSF to each star, using the 37 pixels that are within 3.5 pixels of the star's brightest one. Prior to the fitting, the pixels of each star were normalized to a total of unity. In the PSF that we used, the centermost pixel contained 0.22 of the total flux. Since the figure shows variations of ± 0.02, this constitutes a $\pm 10\%$ change in the value of the central pixel. Any photometric method that concentrates on the core of the image therefore risks errors approaching this size.

This plot resembles the aberration maps shown by Krist (2003). Since chip thickness affects sensitivity as well as charge diffusion, the flat fields also show the same behavior (see the the appendix of his report).

The appearance of Fig. 1 suggests that we need fiducial PSFs at spacings of about 500 pixels. The pattern that we chose is shown in Figure 2. In each of the WFC chips there are 9×5 fiducial PSFs, so that the total array has 9×10 fiducial PSFs. Because of the discontinuity between the two chips, we had to have a fiducial PSF at each of the adjacent edges. Note that the fiducial points are not quite evenly spaced in x; we wanted to have a fiducial point where the PSF has the greatest central concentration (at about $x = 2800$ in the upper chip.) We find that linear interpolation in this grid is adequate.

Using this formalism we constructed each of the 90 fiducial PSFs. Each one consists of an array of 101×101 values for Ψ_{mn}, sampled every quarter pixel in x and y and covering the pixel domain [−12.5:12.5,−12.5:12.5]. We store all these models in a single `fits` image, with the PSFs arrayed in the same order as on the chip. The size of the `fits` image is 901×1001 pixels. Figure 3 shows the layout of such a PSF file.

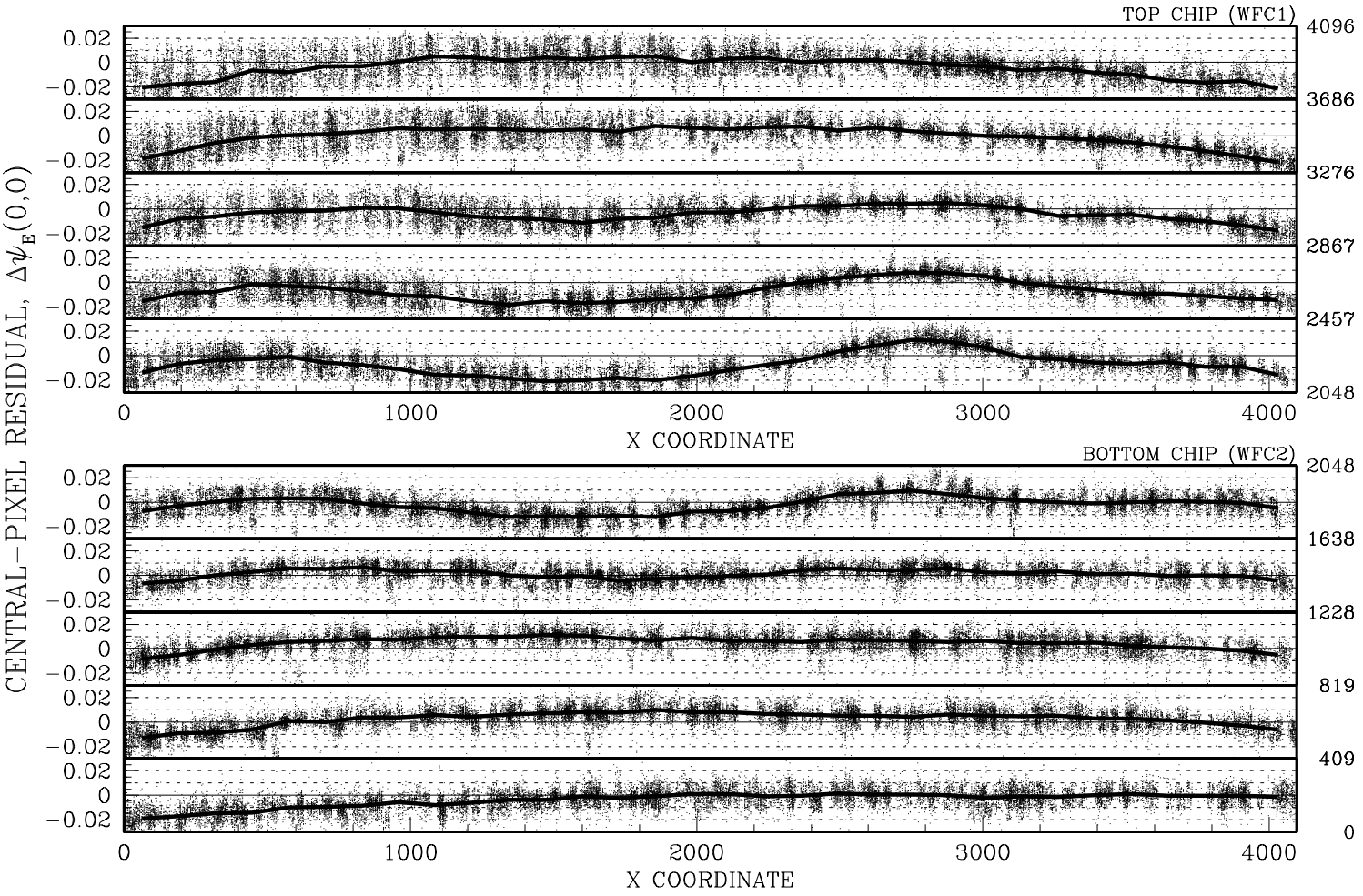

Fig. 1.— Residual in the central pixel of stars, after normalization and subtraction of a fixed PSF. Each dot is an observed star, in one exposure, that falls within the indicated y range for each panel. Dotted lines are drawn at ± 0.01 intervals. The bold lines are running means over 128 pixels in x.

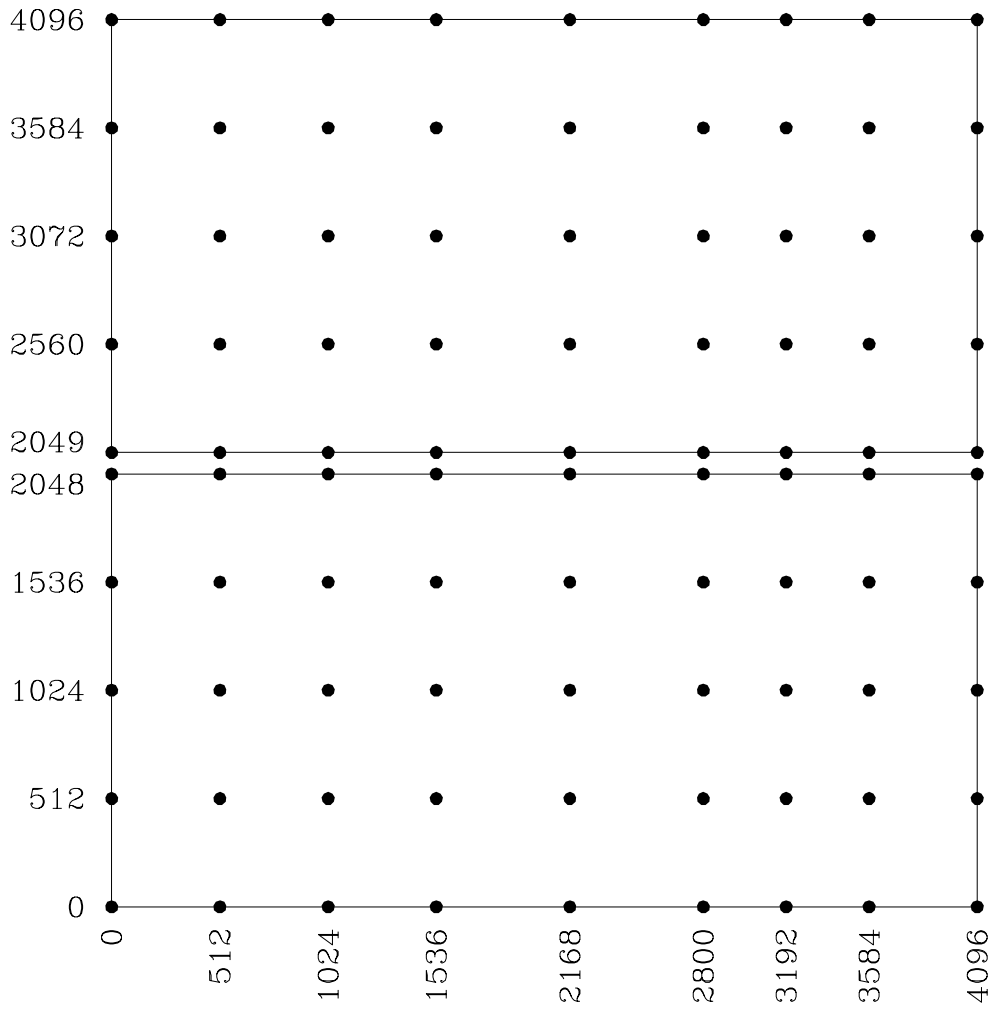

Fig. 2.— The locations of our fiducial PSFs. To construct a PSF at an arbitrary point in the image, we interpolate the PSF among the four nearest grid points.

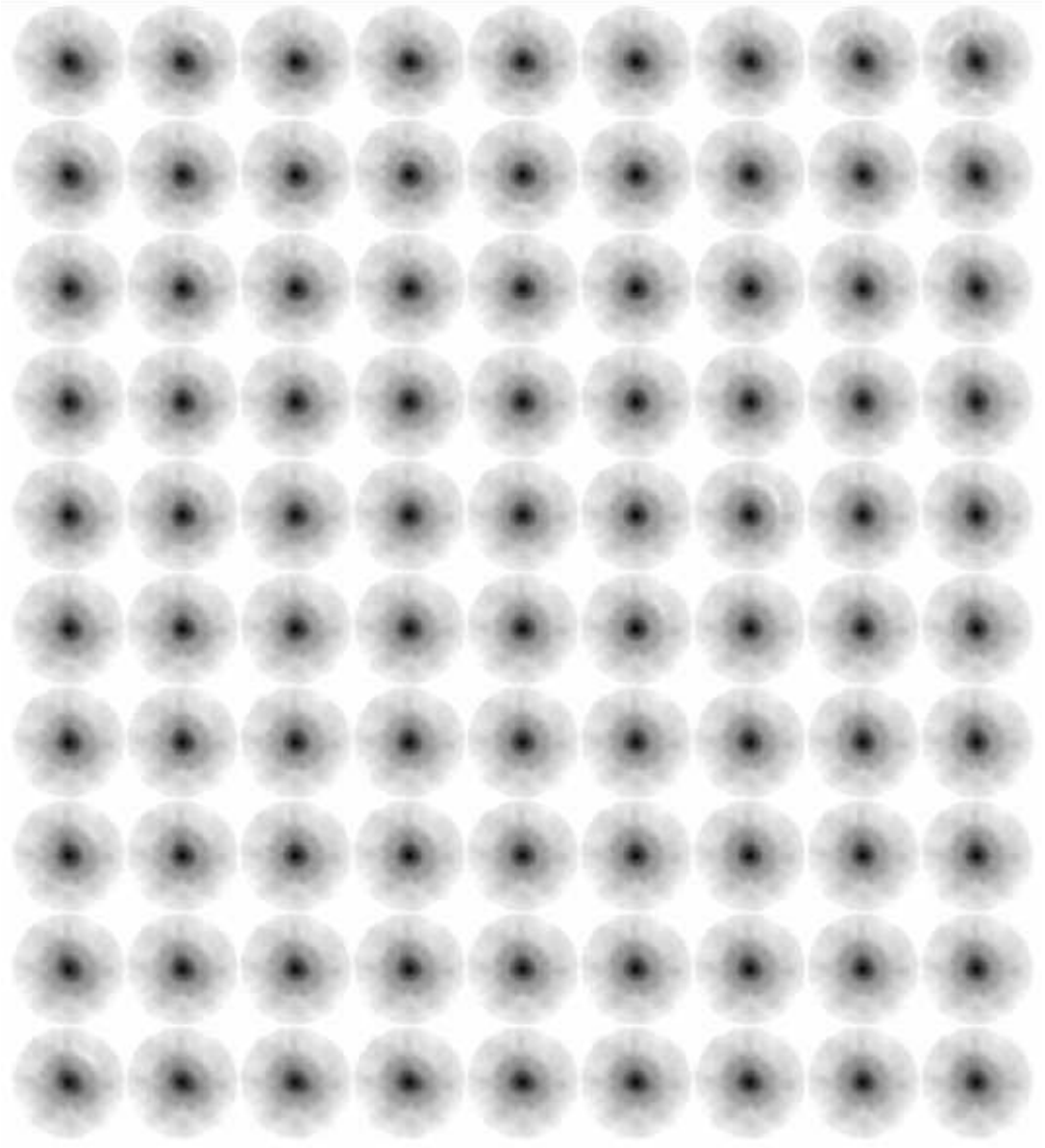

Fig. 3.— The image `PSFEFF.F606W.fits`, showing the array of 9×10 101×101-point ePSFs for the F606W filter.

3.1. Constraints on the PSF models

We will not go into all of the details of how we solved for the PSF; suffice it to say that our approach is very similar to that in AK00 or Anderson & King 2004. What we do describe here are the constraints that keep the PSF physically reasonable. They involve the centering of the PSF, its smoothness, and its normalization. We discuss them briefly below.

3.1.1. Constraint #1: Centering

In the iterative process of fitting the PSF to stars and fitting stars to the PSF, it is possible that the center of any individual PSF could migrate away from the center of its grid, [51,51]. Since our measurement procedure constructs a tailor-made PSF for each star by interpolation within the 9×10 array of fiducial PSFs, it is crucial that these PSFs all be centered in the same way.

Here we used a somewhat different approach from that of AK00, since the undersampling in the WFC is not as severe as that in the WF chips. At each iteration we found the center of each fiducial PSF, by fitting a quadratic polynomial to its inner 7×7 grid points, and shifted it as needed, to restore the center to its proper position at [51,51].

3.1.2. Constraint #2: Smoothness

The derivation of the values at the individual grid points is noisy, whereas the PSF should vary smoothly from point to point. Near the center we smooth with a 5×5 kernel that is equivalent to replacing each value by the value of a quartic whose 15 parameters come from a least-squares solution over the 5×5 Ψ_{mn} array values centered on the one in question. Its coefficients are:

```
 0.0416 -0.0808  0.0784 -0.0808  0.0416
-0.0808 -0.0196  0.2008 -0.0196 -0.0808
 0.0784  0.2008  0.4416  0.2008  0.0784
-0.0808 -0.0196  0.2008 -0.0196 -0.0808
 0.0416 -0.0808  0.0784 -0.0808  0.0416
```

Beyond a radius of 5 image pixels, where the PSF should vary even more smoothly, we used a quadratic kernel. Beyond 10 pixels, we used a linear one; in both cases the fitting

continued to use 5×5 points. Examination of the residuals of fitting the PSF to star images shows that this constraint removes high-frequency noise without suppressing any significant PSF structure.

3.1.3. Constraint #3: Normalization

We normalize our PSFs to have a total flux of unity within a radius of 10 WFC pixels, but this normalization can be a tricky problem. The ePSF, $\psi_{\rm E}$, is a continuous function, but our representation of it, Ψ_{mn}, is discrete; it is a sampling at an array of points that is 4×4 times as closely spaced as the image pixels. If a star is centered exactly on a pixel, the pixel values of the PSF for it will come from the central value of the Ψ_{mn} array and the value of every fourth point in each coordinate direction. To scale the PSF so that its sum within a radius of 10.0 pixels is unity, we sum the values that lie within that radius, and divide the entire PSF by this sum.

Now this normalization does not imply that the corresponding sum for a star that is not centered on a pixel will necessarily be unity. That sum will come from a different set of grid points, and although the grid points are constrained to vary smoothly, they could still have a different sum. In fact, with an undersampled PSF and a sensitivity that is not uniform within a pixel, the total flux recorded by the detector will depend on where the star's core lands in the pixel, and the normalization of the PSF must take this into account.

In AK00, where we were dealing with WFPC2 detectors whose sensitivity was not uniform within a pixel, we required the normalization factors corresponding to different pixel phases to take whatever value the PSF-construction procedure found for them. For WFC, however, we have found that the sensitivity within pixels is uniform; this allows us to require that the PSF sum within 10.0 pixels be unity for all stars, not just for stars that are centered in a pixel.

With the normalization described above, the total PSF flux is unity within 10.0 pixels; but even if we fit a star image within a smaller radius, the flux scaling will still be as if we had fitted out to a radius of 10 pixels. This radius corresponds to 0.″5, the aperture used for calibration by De Marchi et al. (2004) and by Sirianni et al. (2005). We note, however, that we measure fluxes in the `_flt` images, while their calibrations apply to the `_drz` images. To relate the zero points of our PSF-fitting magnitudes to those of the previous calibrations, it would be necessary to measure a number of isolated stars with aperture photometry on the `_drz` images and with PSF fitting in the `_flt` images. We have not carried out that process here.

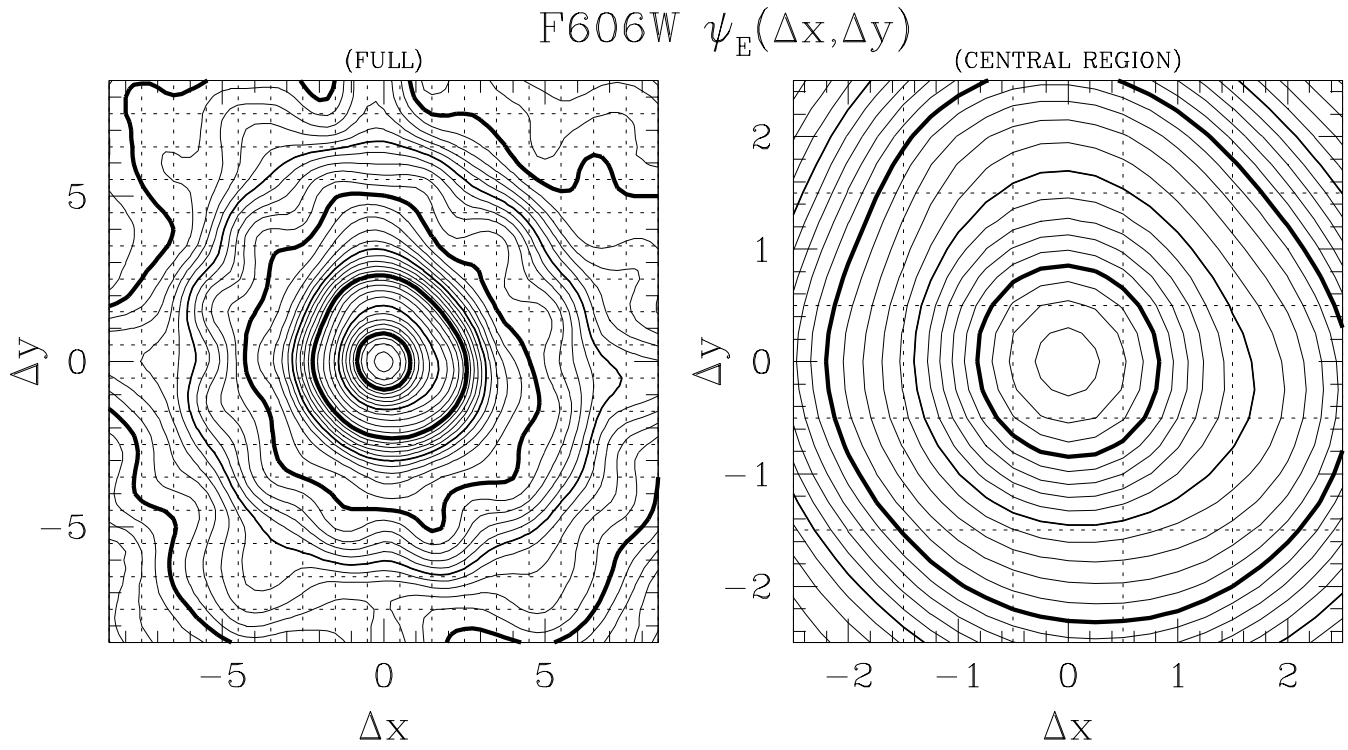

Fig. 4.— Contour plots of the average F606W PSF. The heavy contours correspond to ψ_E values of 0.1, 0.01, 0.001, and 0.0001. The lightest contours have an interval of 0.1 dex. Left: the full PSF over an 8 × 8-pixel span. Right: the central region. The dotted lines have a spacing of one pixel unit.

3.2. The derived PSFs

Figure 3 showed that the fiducial PSFs all look quite similar, to first order. Figure 4 shows a contour plot of the average of the 90 PSFs. The PSF changes by more than two orders of magnitude within the central region (right panel). Our fits to stars are usually confined to this region, since most of the light is there, and since position measurements are most sensitive to the region where the gradients are largest.

Note also that the PSF is quite asymmetric in both the Δx and Δy directions. For this reason, defining a simple FWHM, ellipticity, and orientation would not adequately describe the PSF and its variation.

Just as Figure 3 showed the similarity of the 9×10 fiducial PSFs, in Figure 5 we show their differences. The figure gives a close-up of the central pixels, with the average model subtracted. The core intensity clearly changes dramatically from fiducial point to fiducial

point (note the sharp variations between the 5th and 6th columns). This is almost entirely due to the variations in charge diffusion, related to variations in chip thickness. The region just outside the core (the PSF's inner halo) changes more smoothly from fiducial point to fiducial point. These changes are related to the optical aberrations.

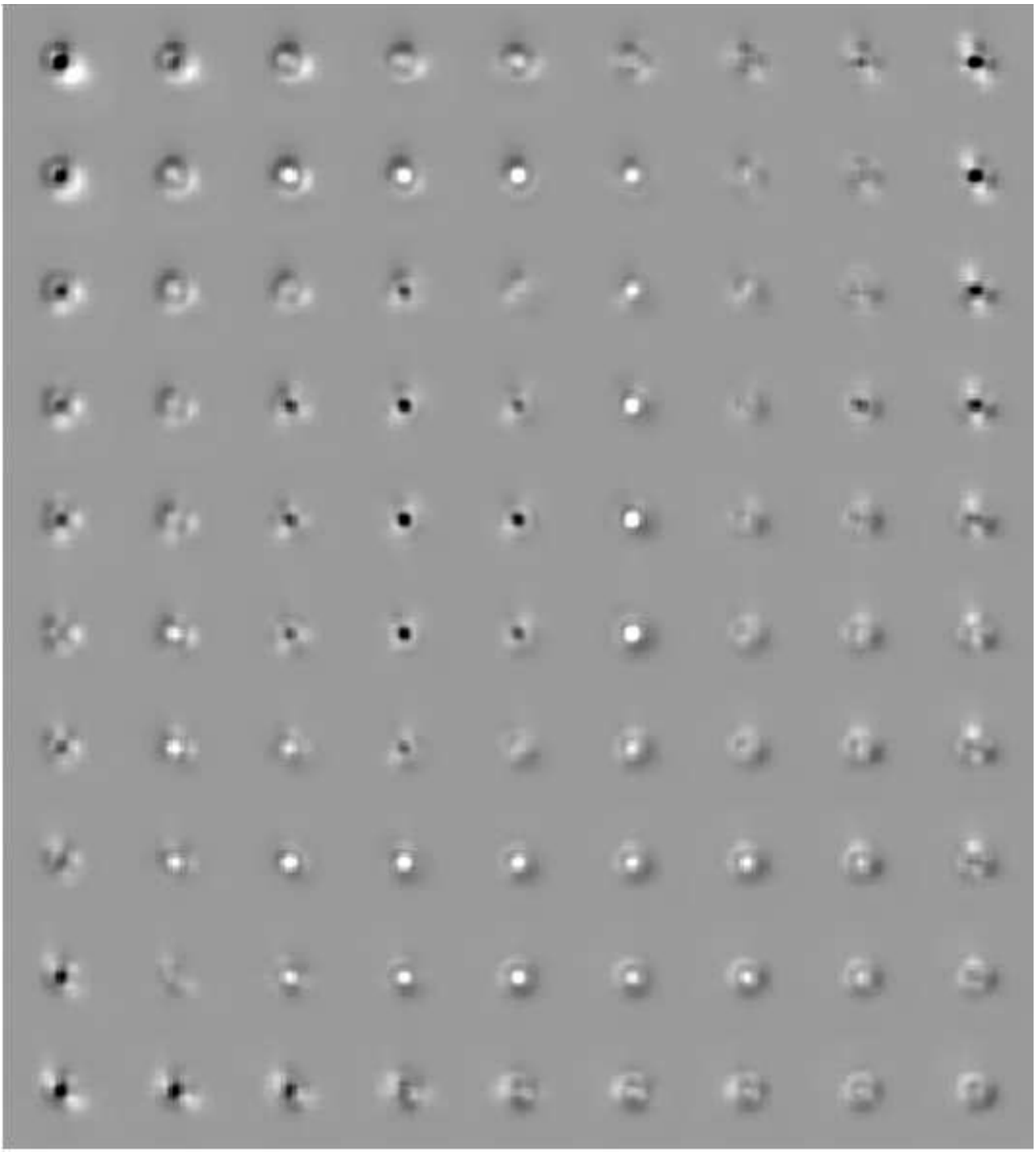

Fig. 5.— The array of 9×10 fiducial PSFs, as in Figure 3, but this time with the average PSF subtracted from each. To focus on the central region, we only show the inner 6-WFC-pixels' radius for each PSF. The whitest pixels indicate an excess of 0.035 and the blackest indicate a deficit of 0.035, a ±15% variation in the PSF's central intensity.

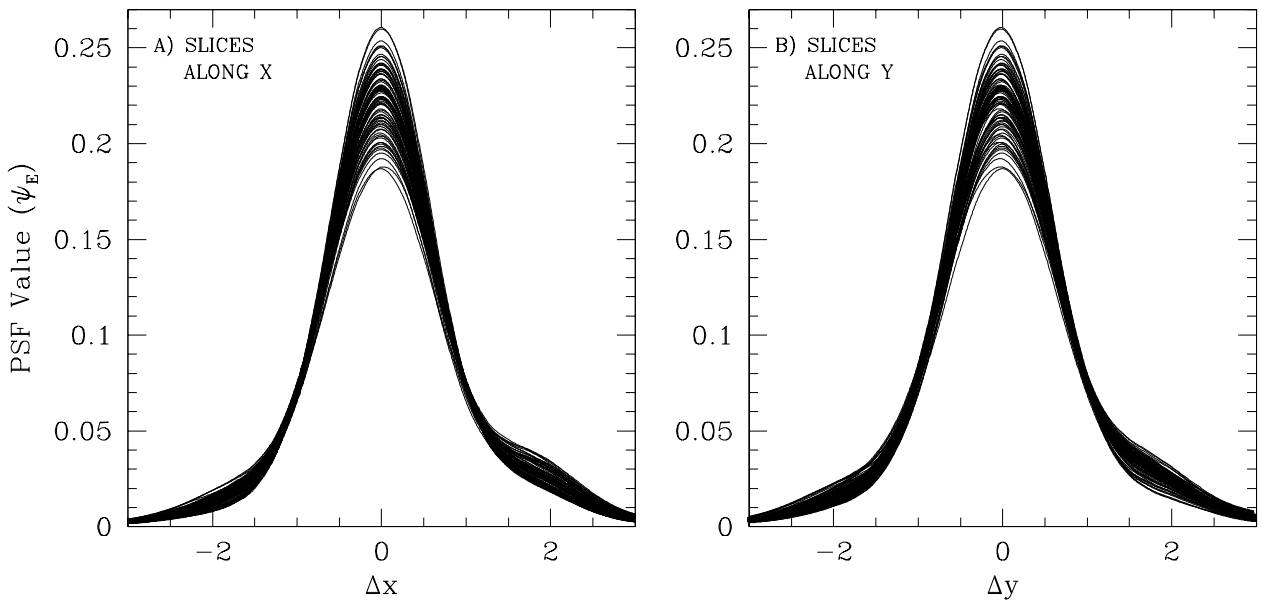

Fig. 6.— The x and y profiles through the centers of all 90 fiducial PSFs.

Since it is hard from gray-scale images to get an appreciation of how much the PSF changes with position, we show in Figure 6 the value of $\psi_{\rm E}$ for slices through the center of the PSF, along x and along y. It is clear that the central value of the PSF varies by more than 10%, and that the amount in the wings can vary by more than 25% in response to changes in the core.

Finally, to show even more quantitatively what the PSF is doing, we list below the central value of each of the 9×10 fiducial PSFs for the F606W filter:

```
0.187  0.211  0.228  0.229  0.233  0.226  0.220  0.214  0.188
0.200  0.230  0.247  0.246  0.250  0.238  0.230  0.221  0.192
0.205  0.232  0.228  0.210  0.229  0.239  0.230  0.225  0.200
0.212  0.227  0.208  0.197  0.215  0.251  0.224  0.213  0.204
0.209  0.228  0.210  0.195  0.204  0.261  0.228  0.223  0.218

0.221  0.238  0.212  0.201  0.214  0.260  0.227  0.229  0.226
0.214  0.242  0.236  0.215  0.229  0.237  0.229  0.231  0.223
0.217  0.239  0.251  0.254  0.244  0.241  0.241  0.234  0.221
0.203  0.224  0.238  0.242  0.245  0.236  0.239  0.234  0.222
0.198  0.199  0.207  0.218  0.224  0.229  0.228  0.229  0.225.
```

The central value of the PSF grid ($\Psi_E[51, 51]$) is the fraction of a star's light that falls

in the central pixel when the star is centered exactly on that pixel. We see that across the chip this varies from 0.187 to 0.261, a factor of nearly 1.4! And the variation of other parts of the PSF can be seen qualitatively in Figures 5 and 6.

3.2.1. Evaluating the derived PSFs

Figure 1 showed that a spatially constant PSF is unable to model the fraction of a star's flux that falls within the central pixel. Figure 7 shows a similar plot for the spatially variable PSF derived above. It is clear that most of the variation has been properly treated. Although this figure shows only the improvement in predicting the flux in the central pixel, the rest of the PSF is similarly well modeled.

We have run some additional tests to verify that these PSFs measure consistent fluxes everywhere on the detector. There is a calibration field in 47 Tuc that has been observed by the WFC through F606W well over 160 times, at a wide variety of offsets and orientations. We measured all the stars in all the exposures, and examined the photometric residuals as a function of position in the detector. Nothing is significant at the 0.01 magnitude level, which means that our photometry and the flat fields are both quite good. We will show the details of this test in the subsequent ISR on the distortion solution.

3.3. PSFs for other filters

All the preceding analysis used only our F606W PSF. In addition we have found well-dithered, well-exposed data sets for F435W, F475W, F625W, F658N, and F814W. The PSFs for these filters can be found on the web site given in Section 5. We will refer to them as library PSFs. In the Appendix, we examine the residuals for the F435W and F814W PSFs and conclude that our 9×10 prescription appears to be adequate for all wavelengths.

Good data sets may exist for some other filters, but we have not found them. If any users have an interest in PSFs for other filters, it would not be hard for us to construct them, given a good data set.

At some point it might be useful to compare our PSFs against those generated by Tiny Tim. We have not made such comparisons, but it would be interesting to see them.

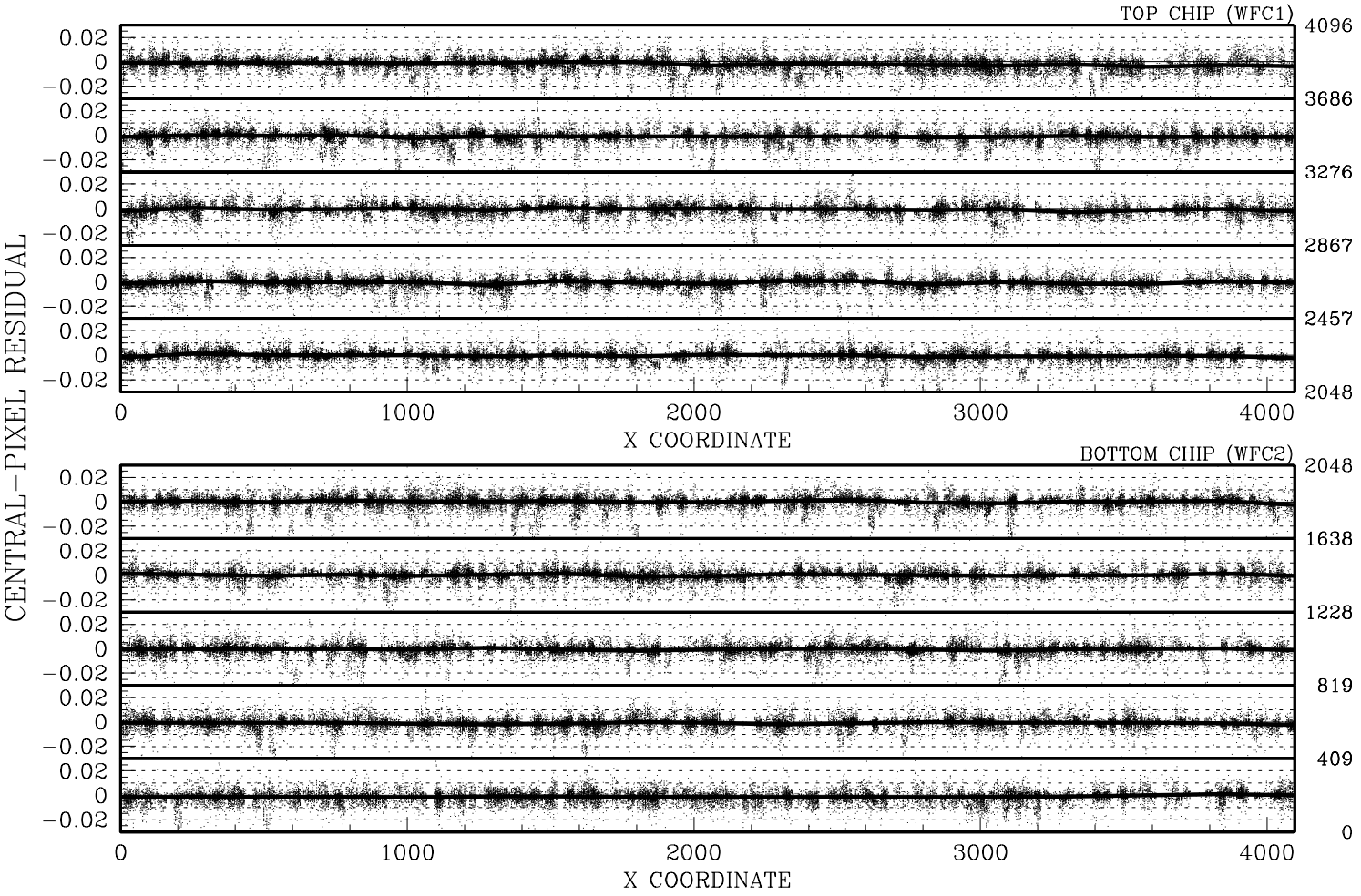

Fig. 7.— Like Fig. 1, but for a spatially varying PSF. The quantities plotted are again the central-pixel residuals of stars, after fitting the PSF to normalized pixel values and subtracting it.

4. Time variability of the PSF

HST PSFs are much more stable than ground-based PSFs, which change dramatically with the seeing. Nonetheless, the WFC PSF does change shape over time in response to instabilities in pointing or changes in focus. The biggest effect that these variations have on the PSF is to change the fraction of flux in the core. Thus the easiest way to look at how much the PSF is changing is to look at how constant its core is.

4.1. Short-term variability

We can examine a set of images taken over the period of a month to see how much the PSF has been affected by variations in focus or pointing stability. GO-10424 observed a field in the globular cluster NGC 6397 over the period from 13 March to 8 April 2005. Each of 126 orbits consisted of a long F814W exposure, a long F606W exposure, and a second long F814W exposure. There are about 4000 well-exposed, unsaturated stars in each exposure, so the data set provides a very good opportunity to study how stable the PSF is over this period.

Figure 8 shows the variation of the central-pixel flux of the PSF as a function of observation date. Zero here represents a baseline value of about 0.22 for the F606W filter (0.19 for the F814W filter). It is clear that the PSF does change over time, but not in a way that is easily characterized. Sometimes it is more concentrated at the end of an orbit, and at other times at the beginning of an orbit. The F606W observations appear to show more PSF variation, with the central pixel going from about +2% to −8% of its average value. For a photometric algorithm that fits only the core, this would introduce an error of 0.02–0.08 magnitude in the absolute photometry. Such an error would manifest itself as a shift in zero point, since a change in the fraction of light in the core would shift the measured flux of all the stars together.

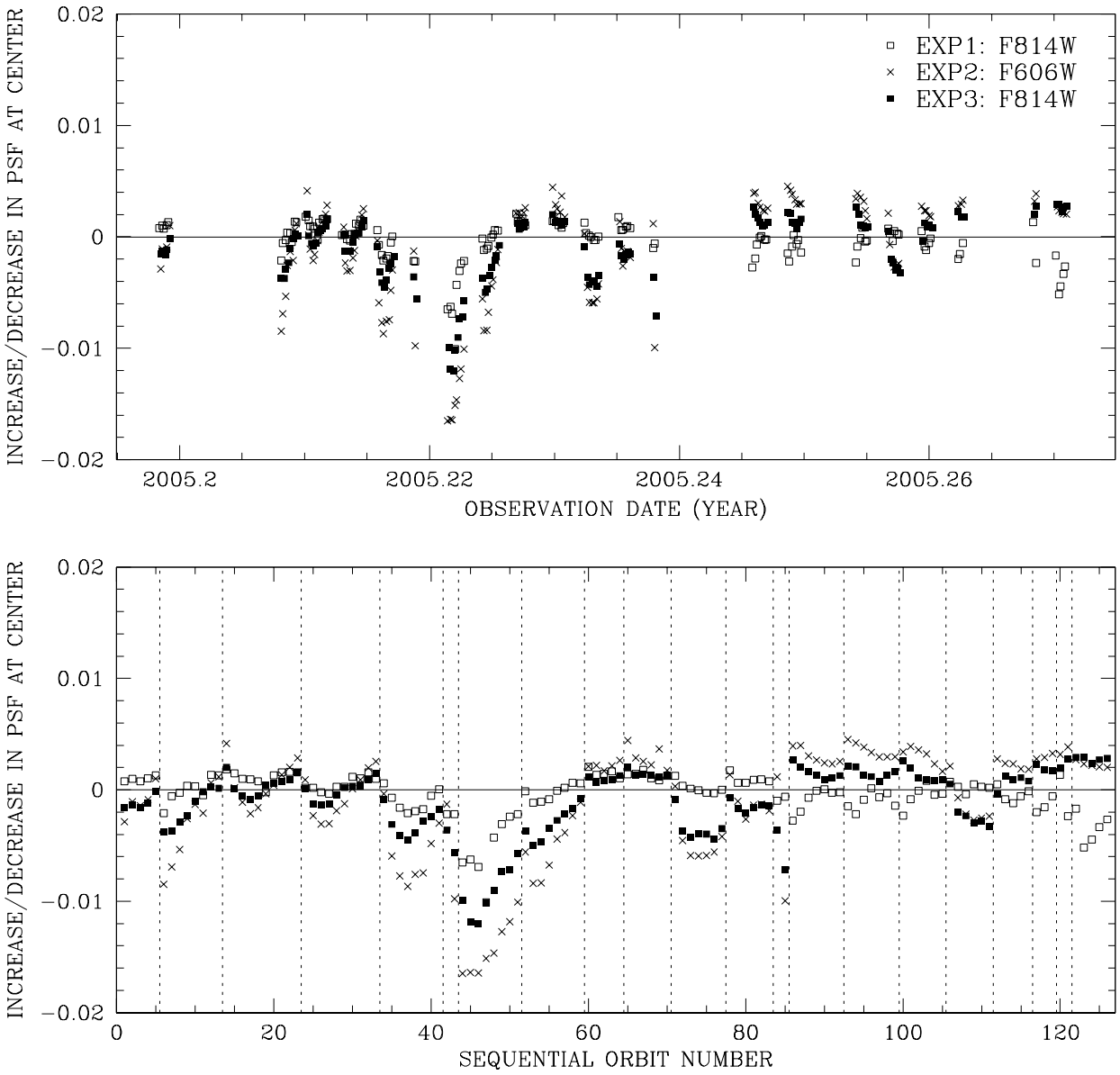

Fig. 8.— The variation of the central-pixel flux in the PSF for the GO-10424 observations of NGC 6397. Top: against observation date. Bottom: against orbit number, with gaps in time indicated by vertical lines. Each orbit consisted of three long exposures: F814W, F606W, and F814W again. A value of 0.01 here represents an increase from 0.22 to 0.23 in the fraction of light in the PSF's central pixel.

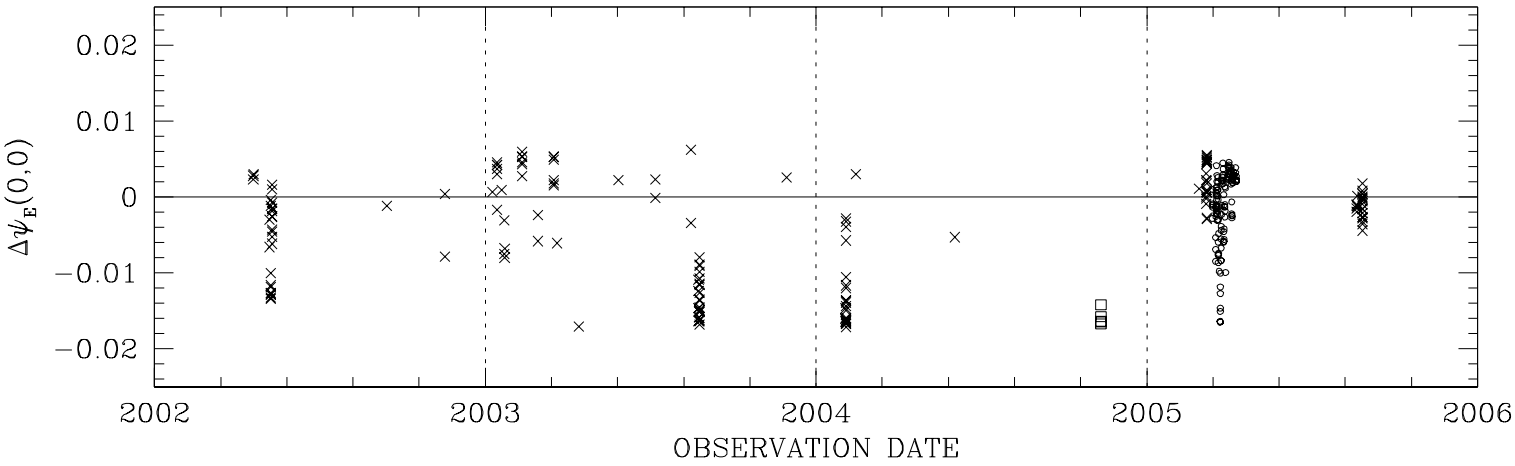

Fig. 9.— The variation of the central-pixel flux over the course of the WFC's orbital lifetime, from the observations of the outer calibration field in 47 Tuc (×'s), from the observations of GO-10252 in Omega Cen (squares), and from the observations of GO-10424 in NGC 6397 (circles).

4.2. Long-term variability

We can also examine other data sets to see how the PSF may change over longer time scales. The 47 Tuc calibration field has been observed over 350 times by the WFC, including over 160 times through the F606W filter. Figure 9 shows how the fraction of flux in the core changes with exposure date. The baseline for this is 0.22; thus the fraction of light in the core can clearly change by over 8%. The box symbols show an orbit taken of ω Cen in GO-10252 just before the WFC focus was adjusted[1]. Ironically, these images were taken to measure accurate PSFs and improve the distortion solution, but they now serve to test the limits of the PSF model in extreme conditions.

4.3. Ways in which the PSF changes over time

Which parts of the PSF change when the core intensity changes? Is this a regular and predictable variation? These are complicated questions to answer, since it is difficult to measure a full 9×10 array of PSFs for a single exposure, even for fields that have a high density of well-exposed stars. If the PSF does not change in a simple and regular way with changes in focus, then it will be impossible to come up with any general answer.

[1]http://www.stsci.edu/hst/observatory/focus/focushistory.html

The first thing we looked at was whether the average variation in the core intensity (shown in the previous figures) described well what was happening everywhere across the detector. We therefore took the softest-focus exposure of GO-10424 (`j97115ssq`, taken on 18 March 2005) and looked at the central-pixel value as a function of position on the detector, much as was done in Figures 1 and 7.

Figure 10 shows how the central-pixel intensity compared with that in our model at different locations. The average value for this image is −0.0165, and most of the image shows a central-pixel flux deficit between −0.02 and −0.01. In particular, we do not see much signature at all of the spatial pattern that is so stark in Figure 1. This means that the temporal variation of the PSF is largely decoupled from the spatial variation that necessitates the 9×10 array of models. This makes sense, since the high-frequency spatial dependence comes from the charge diffusion, a detector phenomenon that is unrelated to focus.

This result suggests that we may be able to represent the PSF as the sum of the library PSF and a small perturbation PSF, which depends on the focus. If we have several stars in the image, we can fit them with the library PSF and construct a perturbation PSF from the residuals.

Figure 11 shows perturbation PSFs for some of the images in the GO-10424 data set. It is clear that most of these PSFs are characterized by a transfer of flux from the core to the inner halo, although some show an asymmetry, which might be due to telescope jitter.

4.4. A more detailed look at PSF changes with focus

We have found that the above decoupled treatment does a good job treating much of the PSF's variation. But is there something even better that we can do? Would it be worth while to allow the perturbation part of the PSF to vary with position as well?

In Figure 12 we examine how the residual PSFs vary with location on the chip for three different exposures: a good-focus exposure, a poor-focus exposure, and a very-poor-focus exposure. The average residual PSFs account for about 75% of the observed variation. The remaining residuals do, however, have some coherent spatial dependence. Furthermore, they appear to show some definite trends with focus. The center and right panels, both taken with a worse-than-average focus, both exhibit similar spatial behavior, but opposite in sense to what is seen on the left for a good-focus exposure.

This suggests that perhaps much of the PSF variation might be empirically modeled

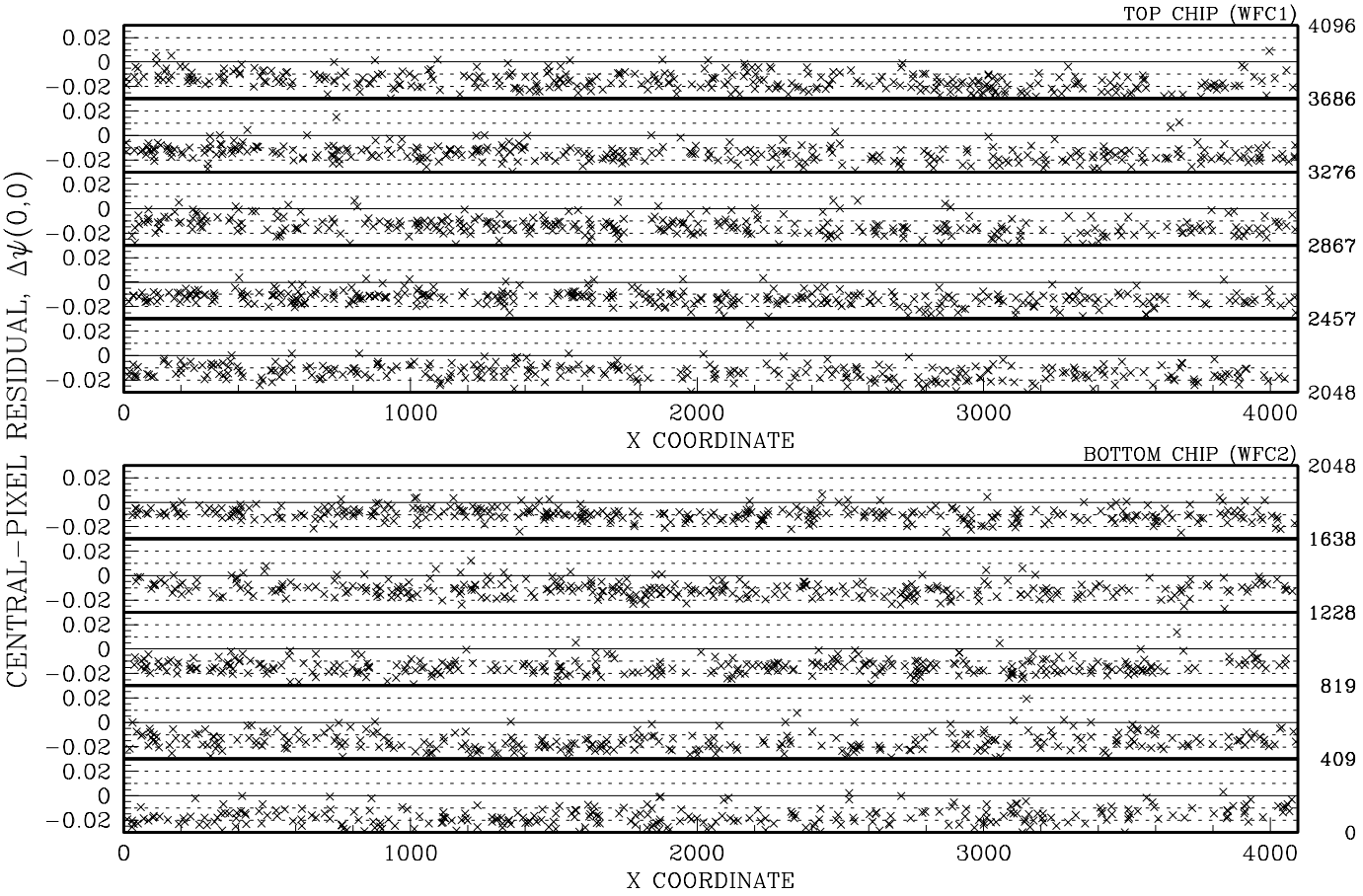

Fig. 10.— The amount of excess/deficit flux in the central pixel for a soft-focus image in GO-10424, as a function of location in the detector. Each × represents a star that was fitted with the spatially variable PSF.

as a one-parameter family. Of course not all of the variation would fit such a model, particularly any variation due to jitter; but some improvements could certainly be made. This might be important for projects that are looking for systematic variations in the shapes of barely resolved galaxies due to weak lensing. For most projects, however, these small PSF variations will be completely unimportant.

4.5. How good a PSF do you need?

Often there will not be enough stars in an image to examine the spatial variations of the PSF in as much detail as we have done here, where we had the luxury of many

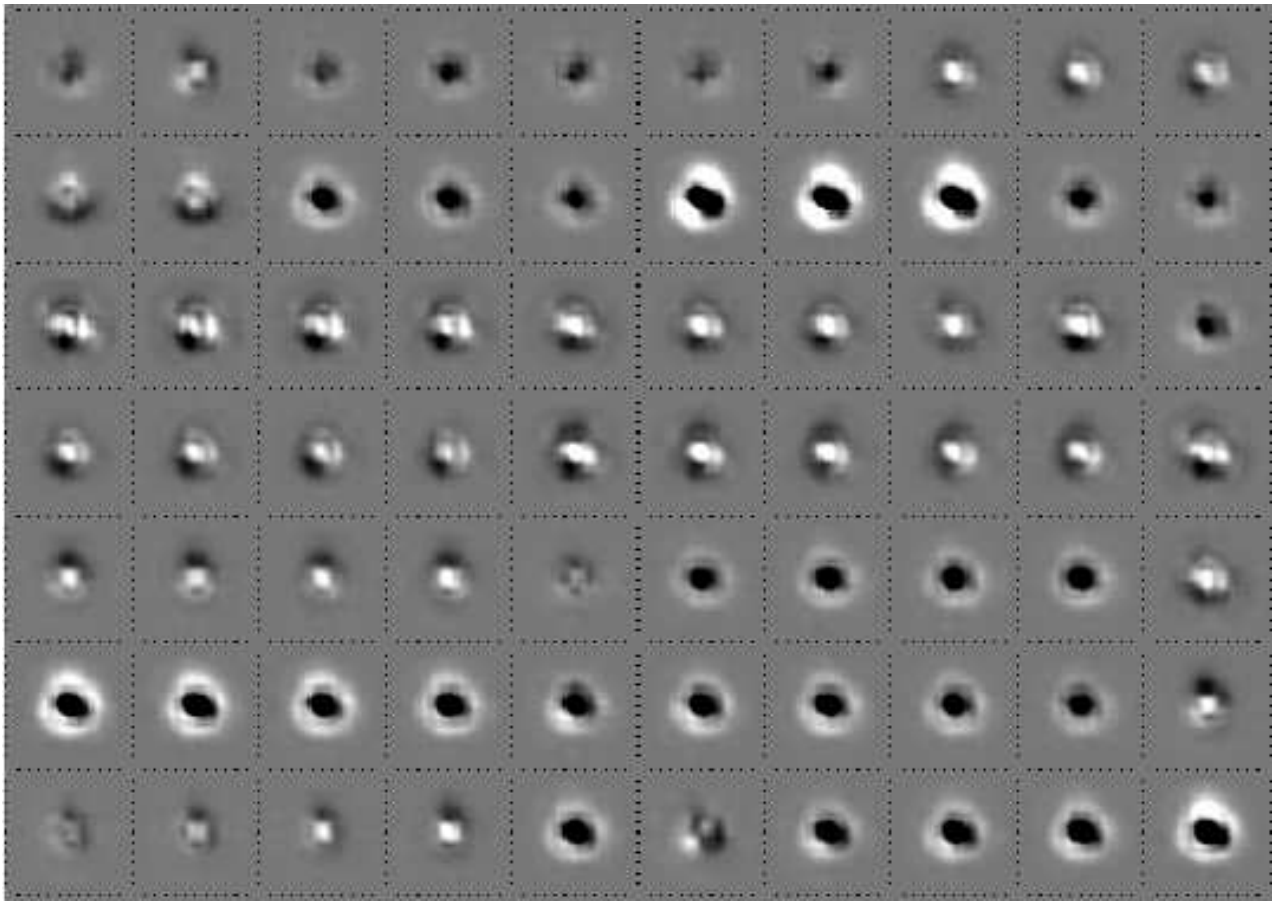

Fig. 11.— The perturbation PSFs for 70 of the images in the GO-10424 data set. Each PSF here represents the difference between the true PSF in the exposure and the library PSF. The perturbation is computed only within a radius of 5 image pixels. Dark represents less flux.

thousands of well-exposed stars in each exposure. With less favorable data sets we must rely on the lessons learned here about how accurate we can expect our PSF models to be.

While it would always be good to have a perfect PSF for every situation, in most cases it is not crucial to have perfect knowledge of the PSF; good knowledge can suffice. But how accurate a PSF do we need for different applications? Below we summarize the various stages of PSF sophistication that you might adopt, and the compromises that are made at each stage.

1) **Spatially constant PSF.** If spatial variation of the PSF is ignored, the PSF will be in error by up to 10% in the core, which can affect photometry at the 0.1-magnitude level, if you are doing core fitting. If you are fitting to a larger aperture, the error will be less

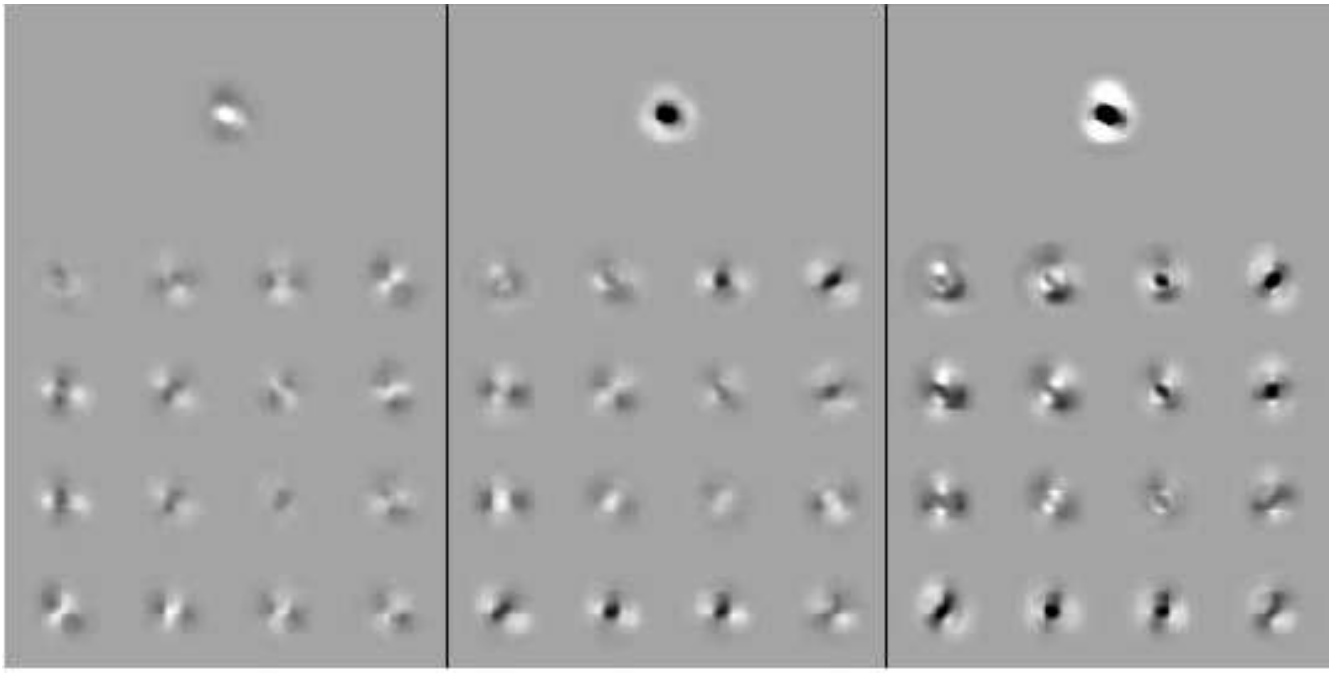

Fig. 12.— For three exposures, the global average perturbed PSF (top), and the residuals from this average for 4×4 regions in the image (below). From right to left, the exposures have $\Delta\psi_{\rm E}(0,0)$ of 0.004, −0.010, and −0.018. The left and center ones come from GO-10424 and the one in the right panel from GO-10252, the program taken just before the focus readjustment.

than this—typically 2 to 3% for an aperture with a radius of 2.5 pixels, and less than 1% for apertures larger than 3 pixels' radius. Astrometry may have spatially dependent systematic errors at the 0.01 pixel level. (Note that if the PSF is not constructed carefully from well-dithered observations, the systematic errors in astrometry could be much larger.)

2) **Library PSF.** If you treat the spatial variability by using one of the library PSFs provided here, but ignore the fact that the PSF can change shape from exposure to exposure, then the PSF model could mis-predict the amount of light in the core by ∼5%. The main effect that this will have is to introduce a zero-point shift of ∼0.02 mag between exposures taken with the same exposure time. A secondary effect will be that faint stars (which are necessarily fitted in the core only) may end up having a slightly different zero-point than the bright stars (by 0.01 mag or so).

3) **Library PSF plus a global perturbation PSF.** This fitting mode can be invoked by setting a flag in the photometry program that is described below. The program needs to have a reasonable number of bright stars to allow it to measure a global perturbation to

the PSF. This will treat most of the PSF variations, but there may still be small errors in the PSF at the edges of the chip (see Fig. 12). The systematic photometric error due to this will probably be less than 0.01 mag.

Reductions for a given project should be done with no more complicated a PSF model than is needed. There is no point in trying to model PSF effects that will have a minimal impact on the results. There may, however, be some projects where a very sophisticated PSF model will be crucial, such as weak-lensing analyses or searches for faint structure around bright sources. Unfortunately, such projects tend not to have enough bright stars to allow construction of an elaborate PSF.

5. Using the PSFs

The PSFs that we provide are all effective PSFs; they tell us what fraction of a star's light should fall in a pixel located at a given offset $(\Delta x, \Delta y)$ from the center of a point source. These PSFs can be used to fit stars both for position and for flux, or to do more complicated operations such as point-source subtraction, extended-source modeling, or even deconvolutions.

5.1. Downloading the material

All the public material referred to in this section can be found in the directories at

`http://spacsun.rice.edu/~jay/WFC.`

There is a directory for PSFs and one for `FORTRAN` routines.

5.2. Measuring stars

A point source has three intrinsic parameters that we can measure: the flux (f_*) and the position (x_* and y_*). The goal in PSF fitting is to find the combination of these three parameters that best describes the distribution of flux in the star's pixels.

5.2.1. A measuring program

In the `FORTRAN` directory we provide a program that takes one of our PSFs and a WFC image and measures all of the sources in that image that qualify under some simple finding criteria. The program returns a list of x, y, and m (instrumental magnitude) for all the "found" sources. One can then use collating routines (see below) to combine and compare positions and fluxes from exposure to exposure.

The measuring program is called `img2xym_WFC.09x10`, because it takes an image, creates an `xym` file, for WFC images using an array of 09×10 PSFs. Its opening block of comments describes its use. The program takes five arguments. The first (`h`) specifies how far away from a brighter pixel an identified peak in the image must be, to be considered worth measuring. The second parameter (`fmin`) allows you to accept or reject sources according to the total flux above sky in the brightest 4×4 pixels. The third parameter

(pmax) allows you to exclude saturated stars, by setting it to 54999 (or 69999 for GAIN=2). (Both of these limits were found empirically by inspection of histograms of _flt pixel values to note what pixel level is indicative of saturation.) If pmax is set above the saturation threshold, the routine will measure positions and fluxes for saturated stars by fitting the PSF to the unsaturated pixels, but with errors for saturated stars that are much larger than those for unsaturated stars. The fourth parameter is the name of the PSF file (e.g., PSF.F606W.fits).

Following the first four parameters, the user can set some flags. "PERT" will tell the routine to find a spatially constant perturbation to add to the PSF in order to account for focus variations and thus better fit the stars. It will show the perturbations in the file LOG.perts.fits. The flag "SUBT" will tell the routine to generate a star-subtracted image. This subtracted image can be examined to verify that the perturbation PSF does a good job fitting the stars.

Following all these parameters, the routine expects a list of image names. These images can be in the pipeline-product _flt format, or they can be in a compressed format that stores the two chips in an abutted, 4096×4096 image using either short or long integers. We have found that images in these formats can be gzipped to 10% of the original _flt image size. Routines to convert _flt images into our abutted format are provided in the FORTRAN directory.

The output of the program is a file that has the image stem plus a .xym extension. The header of this file contains information about the parameter values and the PSF used. It then has one line for each source found, giving the raw coordinates and the fluxes measured in the image. It also generates a .xymc file which contains the distortion-corrected positions and the pixel-area-corrected fluxes. (When there is distortion in images, it is not possible for an image to conserve both flux and surface brightness. The ACS pipeline follows the convention of preserving surface brightness rather than flux. So, to remove this reduction artifact we need to multiply our measured fluxes by the local projected pixel area in order to get true fluxes. See Section 6.1.3 of the Instrument Handbook.)

Note that the program processes all qualifying "sources" as if they were stars. Some of these may be cosmic rays, warm pixels, PSF artifacts, or noise spikes. Since most observations consist of several exposures at different dither positions, we have found it easier to retain these false detections in the individual-exposure star lists, and to weed them out at the collation stage. However, the routine does output a quality-of-fit parameter (qfit) which could facilitate the weeding out of non-stellar objects.

Figure 13 shows the internal astrometric and photometric errors as a function of

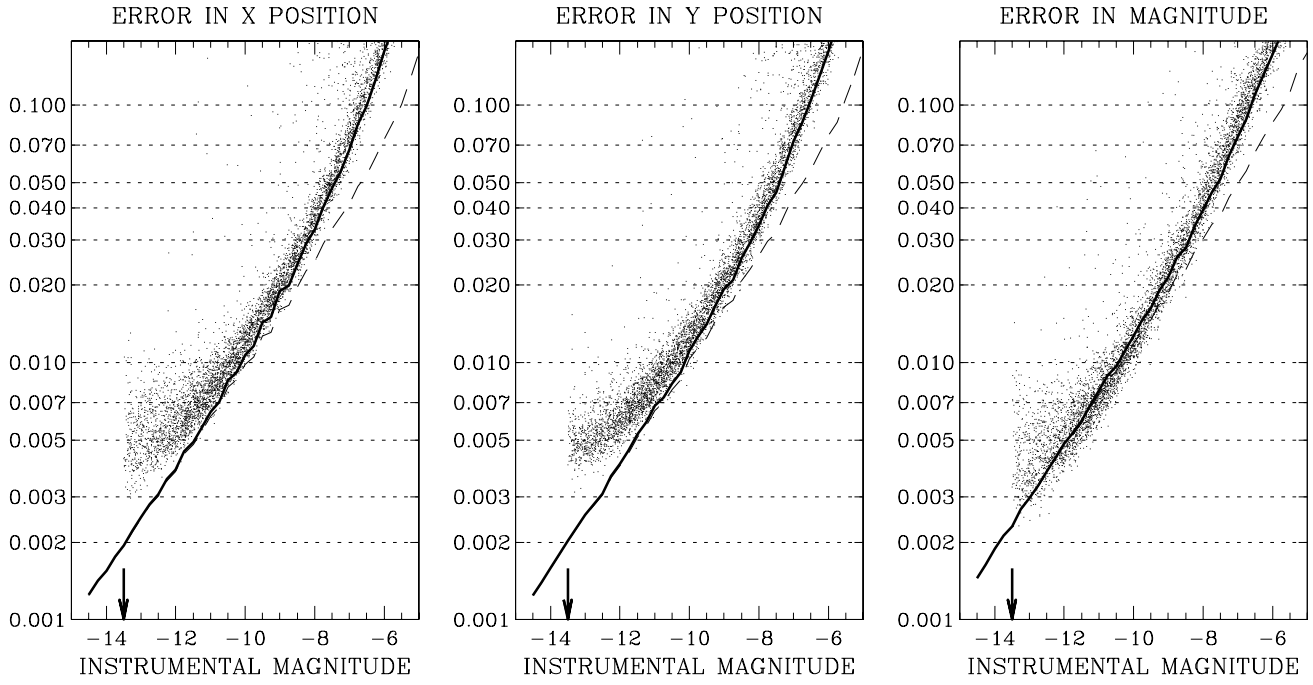

Fig. 13.— Internal photometric and astrometric errors as a function of instrumental magnitude, for the 126 F606W exposures in GO-10424. The error values are residuals from the mean for the star. The heavy line shows the trend from a Monte Carlo simulation using the PSF, with the background value from the image (about 100 electrons). The dashed line shows the simulation for a background of 0. The arrow shows where saturation sets in.

instrumental magnitude, $-2.5\log_{10}(\mathrm{flux_{DN}})$. For the unsaturated stars brighter than -10 (10^4 total counts), we are getting photometry and astrometry better than 0.01 mag and 0.01 pixel, respectively. For the brightest stars, this approaches 0.005 mag and 0.005 pixel in each coordinate.

It is hard to say where the remaining systematic errors are coming from. It is likely some combination of image registration errors, PSF-modeling errors, flat-flat fielding errors, and errors in the distortion solution. The errors shown in this plot represent the error for a single exposure. Multiple observations can be taken in hopes of reducing this error by $\sqrt{N_{\mathrm{obs}}}$, but if all the exposures are taken at the same pointing, any remaining systematic errors will not average away. So, we recommend taking as many different images of the objects of interest as possible, dithering by sub-pixels and whole pixels, and even larger dithers to sample the distortion solution in different places. The optimal strategy will depend on the aims of the project.

5.3. Using the PSFs directly

The `FORTRAN` program `img2xym_WFC.09x10` was designed to measure stars with the PSF models presented here. It may be that users will want to write their own routines to do tasks such as simultaneous fitting of crowded stars, profile fitting for resolved objects, or deconvolution. For this, we provide two ways to access our PSFs directly: a stand-alone program and a subroutine.

The file `gen_locpsf.F` is a stand-alone program that will take as inputs a standard 9×10 library PSF and a location (i, j) in the detector. It will output a super-sampled (×25) version of the PSF that is tailor-made for that location. You can use simple bi-linear interpolation to evaluate it.

If the aim is to measure a large number of objects, it may be awkward to generate a large number of the PSFs using `gen_locpsf.F`. In such a case it might be preferable to use the `FORTRAN` subroutine directly, to evaluate the PSF at each desired location. Within the `gen_locpsf.F` routine there is a simple subroutine named `rpsf_photij.F` that evaluates the PSF directly. Its takes as input the four arguments Δx, Δy, i, and j, and it returns the corresponding PSF value, which represents the fraction of flux we expect in a pixel that is offset by $(\Delta x, \Delta y)$, for a star at (i, j).

We note in passing that if one wants to deconvolve an image, or else fit an analytic function to barely resolved objects, then the effective-PSF formalism provides a natural way to do it. The `_flt` image is simply the convolution of the underlying astronomical scene with the effective PSF. The only limitations are that the observed image contains noise, and is sampled only at the array of pixel centers. This sampling will of course be finer if one has dithered images.

It is worth reiterating that these PSFs are designed for operations on the `_flt` images. This means that the positions and shapes derived with them are in the distorted frame, and must be distortion-corrected to be interpreted in an orthogonal-coordinate space. The ACS x and y axes are inclined at roughly 81° with respect to each other (not the usual 90°), so this can be a very important correction.

Acknowledgements

This research and the writing of this report were funded by STScI grants GO-9443 and GO-10252. We are grateful to Harvey Richer for allowing us access to the images of GO-10424 while they were still proprietary.

References

Anderson, J., & King, I. R. 2000, PASP, 112, 1360

Anderson, J., & King, I. R. 2003, PASP, 115, 113

Anderson, J. 2003, in HST Calibration Workshop Proceedings, eds. S. Arribas, A. Koekemoer, & B. Whitmore, (Baltimore: STScI), p. 13

Anderson, J., & King, I. R. 2004, ACS ISR 2004-15

De Marchi, G., Sirianni, M., Gilliland, R., Bohlin, R., Pavlovsky, C., Jee, M., Mack, M., van der Marel, R., & Boffi, F. ACS ISR 2004-08

Krist, J. 2003, ACS ISR 2003-06

Sirianni, M., et al. 2005, PASP, 117, 1049

APPENDIX

The CCD thickness variations, and resulting differences in charge diffusion produce rather different signatures in the blue and red. Since the bulk of this work involved the more neutral F606W filter, we consider here whether the resolutions adopted are sufficient to capture changes in the F435W and F814W filters.

To this end, we took the library PSFs that we generated for the F435W and F814W filters and used them to fit stars in about 30 images taken of the 47 Tuc calibration field. Many of these images were taken in GO-9018, but some were taken in subsequent calibration programs.

For each image, we found a global perturbation PSF, which typically had an adjustment of about 0.01 (5%) in the central pixel. Next we fit this library-plus-perturbation PSF to each bright unsaturated star in the image, then computed the central-pixel residual to see how well the model predicted the star's flux in its central pixel.

Fig 14 shows the central-pixel residuals as a function of location in the chip for the constant-PSF model (left), and for the 9×10 array of models for the F435W filter (right). The fraction of the total PSF flux in the central pixel is about 0.22, thus a variation of 0.02 corresponds to a 10% variation. The left plot shows that the raw PSF itself is seen to vary by about ±0.02, with a pattern similar to what was seen for F606W. The heavy line shows the trend averaged over 256-pixel-wide bins.

On the right we see that the model does a good job predicting the central-pixel flux. Residual variations are generally less than 0.005, or 2.5%. There does not appear to be any remaining variation at a scale finer than the sampling of the model. It could be that the F435W model could be improved in a few places, as the data set we used to solve for this PSF was not ideal, but the spacing of the array is not a limitation to the model fitting.

Fig 15 shows the same residuals as the previous figure, but this time for the F814W data set. The data set used to construct the library PSF for F814W was much better than that used for F435W, so there are almost no remaining trends in the 9×10 residuals.

So, we conclude that the 9×10 array of PSF models should be able to treat the spatial variation of the PSF for all filters.

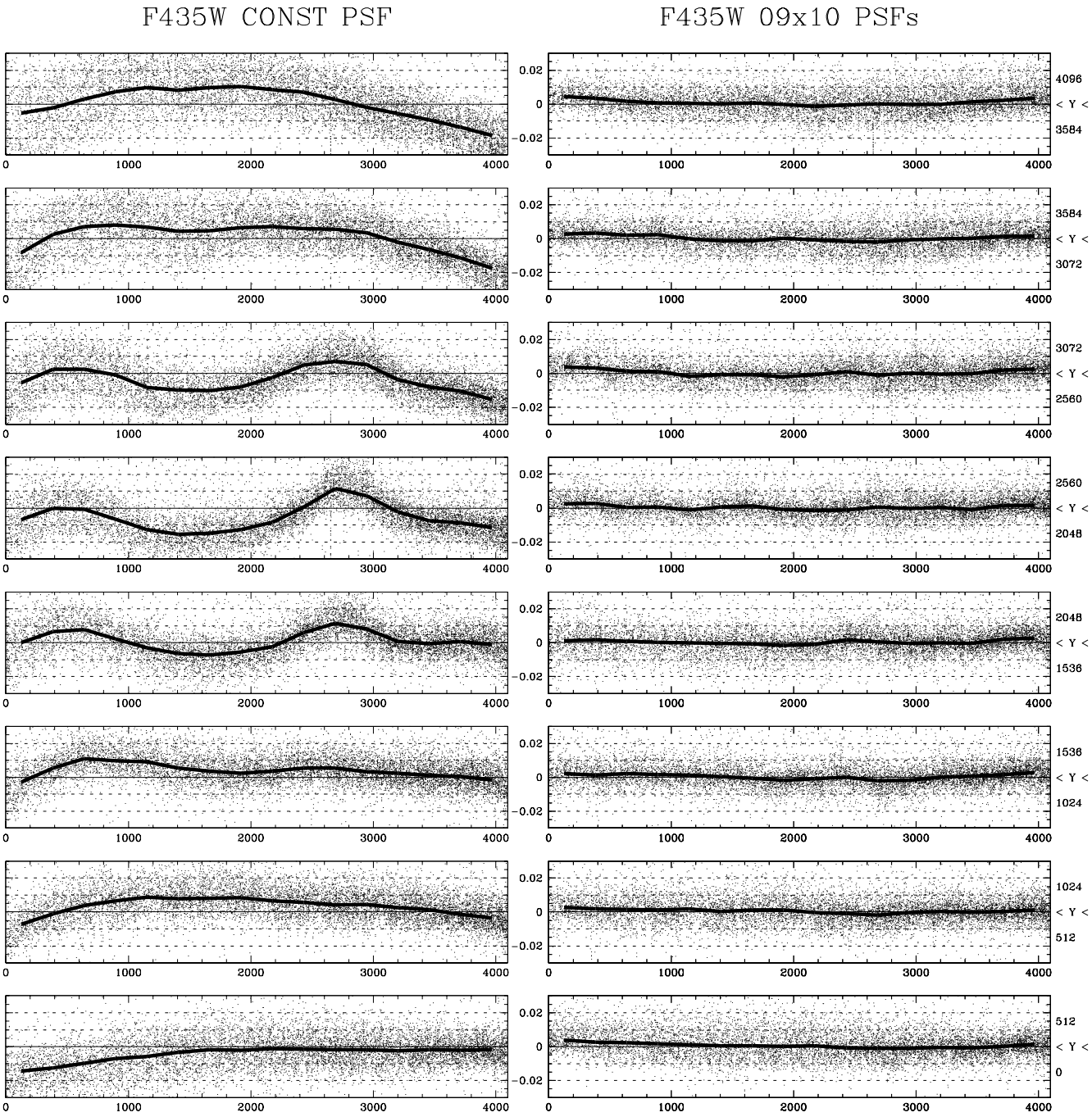

Fig. 14.— Plot of central-pixel residual as a function of x coordinate for 8 horizontal slices throught the image. On the left, we show the results for a PSF that does not change shape with position, and on the right for our library variable PSF. These plots are is similar to Figures 1 and 7, but for the F435W filter.

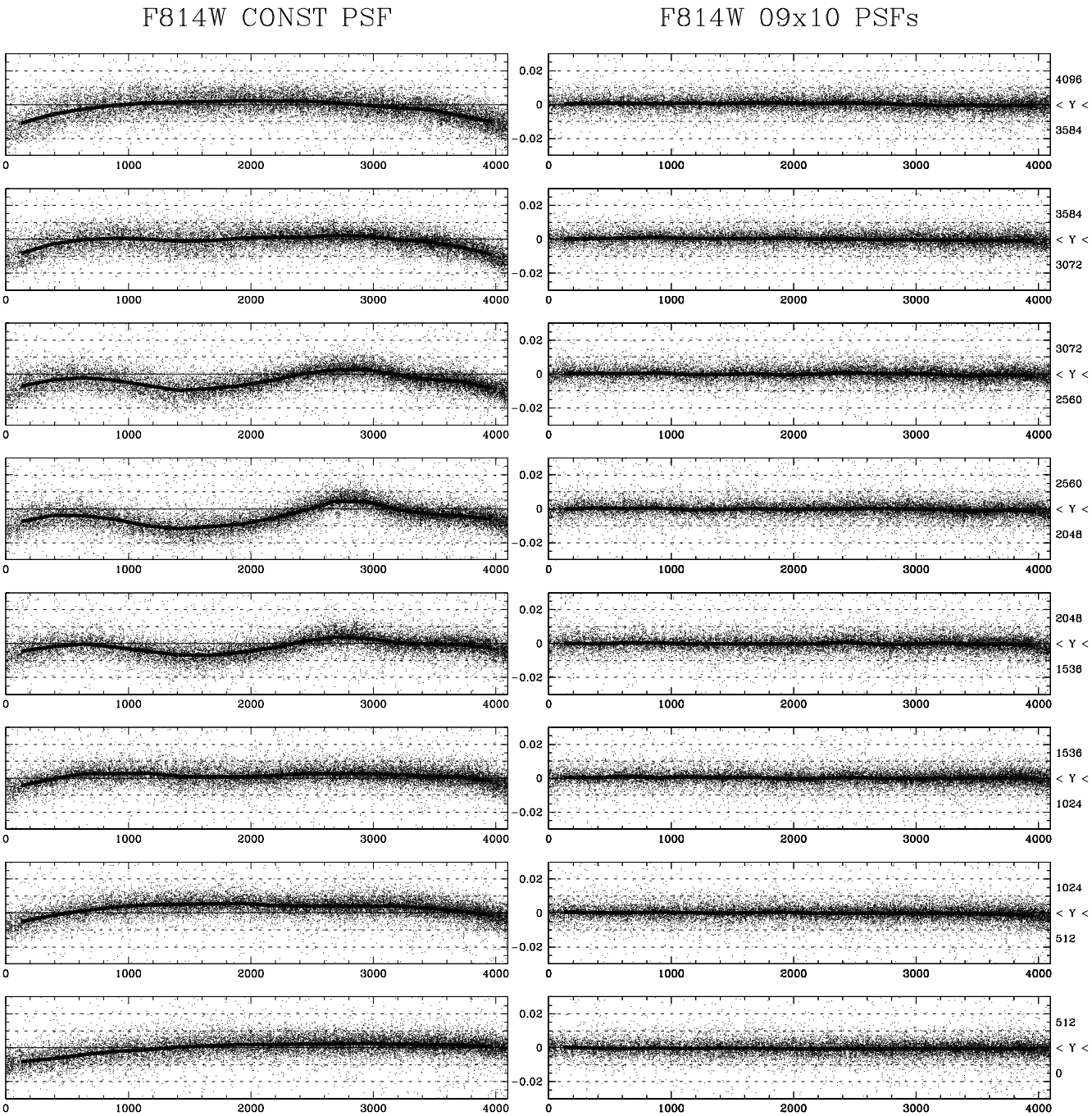

Fig. 15.— Plot similar to Figures 1 and 7, but for the F814W filter.